Evaluation of freeze–thaw damage in concrete by ultrasonic imaging

M. Molero [a,*], S. Aparicio [a], G. Al-Assadi [b], M.J. Casati [c], M.G. Hernández [a], J.J. Anaya [a]

[a] Centro de Acústica Aplicada y Evaluación No Destructiva, CAEND, (CSIC-UPM), Arganda del Rey, 28500 Madrid, Spain
[b] Departamento de Ingeniería Civil y Construcción, ETSICCP, UPM, 28040 Madrid, Spain
[c] Departamento de Vehículos Aeroespaciales, EUIT Aeronáuticos UPM, 28040 Madrid, Spain

This work studies the use of ultrasonic imaging as an evaluation tool in concrete subjected to freeze–thaw (F–T) cycles. To evaluate the damage in this deterioration process, ultrasonic velocity and attenuation images have been generated from concrete specimens with and without air-entraining agents. Two parameters have been proposed from these ultrasonic images according to our experimental setup: the non-assessable area proportion (NAAP) and a weighted average velocity in terms of the NAAP. The proposed parameters have been compared with the recommended failure criteria of the ASTM and Rilem standards, which employ ultrasonic contact measurements. The principal advantage of the use of ultrasonic images and the proposed methodology in comparison with the ultrasonic velocity measurements by contact is the possibility of detection of incipient damage caused by accelerated freeze–thaw cycles.

1. Introduction

Freeze–thaw (F–T) damage is one of the major problems of concrete in cold climates. Cracking and spalling of concrete are the most common damages by frost action, caused by progressive expansion of the cement paste matrix from reiterated F–T cycles [1]. Several theories have been proposed to explain this type of damage, such as the hydraulic pressure [2], the osmotic pressure [3] and the micro-ice-lens model [4] among others. The damage by frost is mainly studied in a laboratory by accelerated F–T cycles. Although no evident relationship has been found between the effects induced by accelerated F–T cycles and those induced by F–T cycles under environmental conditions, researchers continue to study F–T damage using accelerated F–T cycles. Different standards have been developed to evaluate the resistance of concrete subjected to accelerated F–T cycles, such as UNE 12390-9 [5], ASTM C666/C666M-03 [6], prENV-9 [7], JIS A 1148-2001 [8], Rilem TC 176-IDC [9,10], and SS13 [11]. However, these standards differ in the testing method used and in the methodology carried out for evaluating damage in concrete specimens. Concrete resistance to F–T damage is usually evaluated and classified depending on the type of damage, whether external or internal. For instance, the standards used in [5,7,11] evaluate external damage and scaling by the loss of mass of material, whereas internal damage is usually evaluated by the ultrasonic pulse transmission time (UPTT) [9,10] and the fundamental transverse frequency measurements [6–9].

The standards that use ultrasonic non-destructive techniques to evaluate the deterioration of building materials are limited to the ultrasonic velocity measurements obtained, which are commonly performed manually. Thus, the lack of automation involves a limitation on the number of measurements performed, resulting in an expensive and unattractive method to obtain images.

Some years ago, the evaluation of concrete structures and cementitious materials by acoustic imaging, as well as the use of the attenuation and velocity measurements at each point of the material, became an attractive solution to provide the identification of irregularities and defects. For example, measurements of velocity, amplitude, and peak of frequency were used to evaluate the damage of concrete by F–T cycles in specimens along various lines [12]. However, the design of equipment to generate images that evaluate the quality and deterioration state in concrete specimens is neither direct nor obvious.

Several methods can be applied to provide high-resolution images of concrete areas, especially for detecting and locating holes, ducts, cracks, and thickness measurements, such as the synthetic aperture focusing technique (SAFT) and tomography techniques [13–15]. Recently, Chai et al. proposed a tomography technique for concrete evaluation using Rayleigh waves [16]. However, there is still a need to develop suitable systems of acoustic imaging to evaluate the deterioration of concrete structures.

The evaluation of deterioration process in cementitious materials using ultrasonic methodologies, and the development of

* Corresponding author.
E-mail address: miguel.molero@csic.es (M. Molero).

methods to generate images that allow the evaluation of material properties, are a part of the research lines of the authors [17–19]. The ultrasonic images allow the identification of irregularities and defects as well as the extraction of parameters, such as attenuation and velocity profiles, at discrete points of the material. The aim of this article is to use an automated ultrasonic imaging system, developed and patented by the authors [20], allowing the inspection of cylindrical samples of cementitious materials. In this case the system was used to evaluate the deterioration in cylindrical concrete samples subjected to F–T cycles. Two groups of concrete specimens, one of them with air-entraining agents, were subjected to accelerated F–T cycles. Ultrasonic contact measurements and automated ultrasonic immersion inspections were conducted in both groups of concrete specimens before and after the cycles. By means of the automated inspection system, ultrasonic images of velocity and attenuation were generated, allowing the comparison of degradation state in the specimens before and after the F–T cycles. Furthermore, from these ultrasonic images, two parameters were proposed to evaluate damage in the concrete specimens using the automated scanning systems designed by the authors. The proposed parameters were compared with the failure criteria of the ASTM and Rilem standards.

2. Failure criteria of standards

The frost resistance of concrete can be assessed using different criteria based on the loss of strength, weight change, dilation, fundamental frequency and ultrasonic pulse transmission time. This study addresses the failure criterion based on only the ultrasonic velocity measurement before and after the F–T cycles.

The standard ASTM C 666 [6] provides a failure criterion using the durability factor, D, which is calculated as

$$D = \frac{(\mathrm{RDME})N}{300} \tag{1}$$

where N is the number of F–T cycles necessary to reach a proposed critical value of the relative dynamic elasticity modulus (RDME; threshold, e.g., 60% according to [6]). If RDME remains higher than this critical value after ending the 300 F–T cycles, then N can be set to 300 [6]. Thus, RDME is computed as [21,22]

$$\mathrm{RDME} = \frac{V_n^2}{V_0^2} \times 100 \tag{2}$$

where V_n and V_0 are the longitudinal velocity at n and zero F–T cycles, respectively.

The Rilem recommendation [9,10] evaluates the internal damage in concrete by the relative ultrasonic pulse transmission time (relative UPTT). However, in this paper, instead of using the relative UPTT, its equivalent in velocity is used, that is, the relative velocity. This relative velocity, RV, is defined as

$$\mathrm{RV} = \left(\frac{V_n}{V_0}\right) \times 100 \tag{3}$$

According to these standards, the failure criteria to assess damage are outlined in Table 1.

The failure criteria shown in Table 1 are compared with the results obtained by the proposed ultrasonic imaging technique in Section 5.

3. Experimental design

3.1. Materials

Two groups of seven cylindrical specimens ($300 \times 150\ \mathrm{mm}^2$) were formed using HA-30 concrete, with only one group possessing air-entraining agents. The materials used were of Portland cement type CEM I 42.5R, normal river sand (0–5 mm) with 2.71 fineness module, crushed limestone aggregates (5–20 mm) with 6.96 finesse module, and ViscoCrete superplasticizers 3425 to improve workability. The air-entraining agent used was Aer 5 with a proportion of 0.022% of cement weight. The proportion of HA-30 concrete is outlined in Table 2.

The specimens were manufactured according to the standard UNE 12390-2 [23]. Subsequently, the specimens were cured in a climate chamber (DYCOMETAL CCK-40/1000) at a temperature of 30 °C and a relative humidity of 37% for 28 days. These selected curing conditions responded to the summer conditions in Madrid (Spain) [24]. In total, there were two groups of seven specimens: HA-30/00-0-6 corresponding to HA-30 concrete specimens without air-entraining agents and HA-30/05-0-6 corresponding to HA-30 concrete specimens with air-entraining agents.

3.2. Freeze–thaw cycles

The specimens were subjected to accelerated F–T cycles according to the standard ASTM C 666 [6], but were adjusted to the curing conditions specified earlier. The trial consisted of 300 accelerated cycles of 4 hr each, between 10 and −17 °C, as shown in Fig. 1. Two experiments were performed to study the two concrete groups of specimens. The duration of a complete experiment was approximately 50 days. The HA-30/00-0 and HA-30/05-0 specimens acting as reference were not subjected to the process of degradation; these samples were stored in a curing condition of 20 °C and 50% relative humidity.

4. Non-destructive testing by ultrasound

The damage caused by accelerated F–T cycles was evaluated using ultrasonic measurements by the contact method and automated immersion inspections, both operated in a through-transmission mode. These ultrasonic measurements were made before

Table 2
Concrete mix proportion HA-30.

Material	Cement (kg)	w/c ratio	Sand (kg)	Aggregates (kg)	Water (l)	Superplasticizers (% of cement weight)
amount/m^3	381.1	0.5	879.99	936.4	190.55	0.60

Table 1
Failure criteria for the assessment of the frost resistance of concrete.

Rilem TC 176 criteria	Not deteriorated	Possibly deteriorated	Deteriorated	Severely deteriorated
Relative velocity (RV)	> 100%	90–100%	80–90%	< 80%
ASTM C 666 criteria	**Frost resistant**	**With Passable frost resistance**	**With Unproven frost resistance**	**Non-resistant to frost**
Durability factor D (RDME when N=300)	≥ 80%	≥ 60%	< 60%	≤ 40%

and after the cycles in all the specimens. The contact method is the technique proposed for its use in standards [6,9,10]. To evaluate the F–T damage using automated inspections, two different ultrasonic scanning systems were used for automated data acquisition and imaging (radial and axial scanning; see Fig. 2). The automated inspections in immersion provide uniform insonification during the scanning by the ultrasonic transducers, involving precise measurements as well as optimizing the number, distribution, and duration of the inspection. The description of these automated systems is presented in Sections 4.2 and 4.3. It is worth noting that the ultrasonic radial scanning system was used to inspect all cylindrical specimens, whereas the axial scanning system was used to deepen the evaluation of damage by F–T cycles in 5 slices of 50 mm thickness from the HA-30/00-2 sample.

4.1. Ultrasonic velocity measurements by the contact method

To calculate RV and RDME, the travel time of longitudinal ultrasonic waves through the specimens was measured using a contact ultrasonic instrument (TICO equipment) with transducers of 54 kHz (diameter of 50 mm) emitting in longitudinal mode and a semifluid as the coupling material. The measurements were made on the central point of the specimens based on the assumption that the dimensions of the specimens remain constant throughout the experimental test. This assumption may not be correct in some cases, but the method is valid to compare the relative dynamic modulus of different specimens with the same dosage of concrete [6]. Before each measurement, the equipment was calibrated using a standard aluminum cylinder.

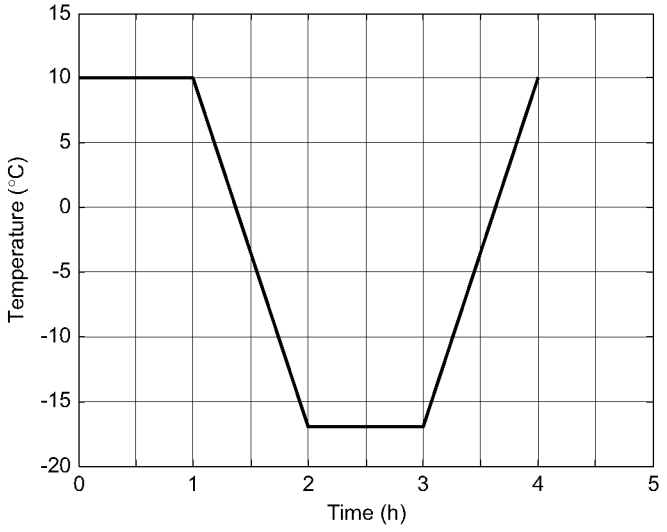

Fig. 1. Accelerated freeze–thaw cycle.

4.2. Ultrasonic radial scanning system (immersion inspections)

A portable ultrasonic inspection system in immersion was designed for automated data acquisition and imaging, see Fig. 2a, by the research group [20]. This system involves the use of a portable immersion tank and two transducers, T1 and T2 (Panametrics v413, 500 kHz) in a through-transmission mode. This system provides two different motions, a rotation centered on the axis of the measuring cylinder and a movement along the specimen's height (see Fig. 2a).

Each pixel of the generated images corresponds to a diameter of a given specimen's height. The complete specimen inspection takes around 10 min with a scanning grid 5 mm in height and a 2° diameter step. The SENDAS ultrasonic system was used to generate and receive the signals. Thus, 10304 A-scan signals were acquired for every specimen with a frequency sampling of 20 MHz. With these A-scan signals, both the amplitude and the time-of-flight were measured to generate the attenuation and velocity maps of the surface or internal features of the specimens. A double zero-crossing algorithm was used to calculate the phase velocity in the specimens [25]. This algorithm can reduce the influence of the received signal amplitudes on the velocity measurements, unlike conventional systems for measuring ultrasonic velocity in concrete.

The ultrasonic velocity of the concrete samples was determined as

$$V_l = \frac{X_c}{t_c - t_{water} + (X_c/V_{water})} \tag{4}$$

where X_c represents the path length of the specimen, t_c is the traveling time of the signal through the specimen, t_{water} is the traveling time in water (with the specimen absent), and V_{water} is the velocity in water at inspection temperature. The attenuation coefficient (α), expressed in dB/m, was computed as the quotient of the maximum amplitude of the received pulse traveling through the specimen, A_s, to the received pulse that travels solely in water, A_w, as:

$$\alpha = 20\ \log_{10}\left(\frac{A_s}{A_w}\right) \tag{5}$$

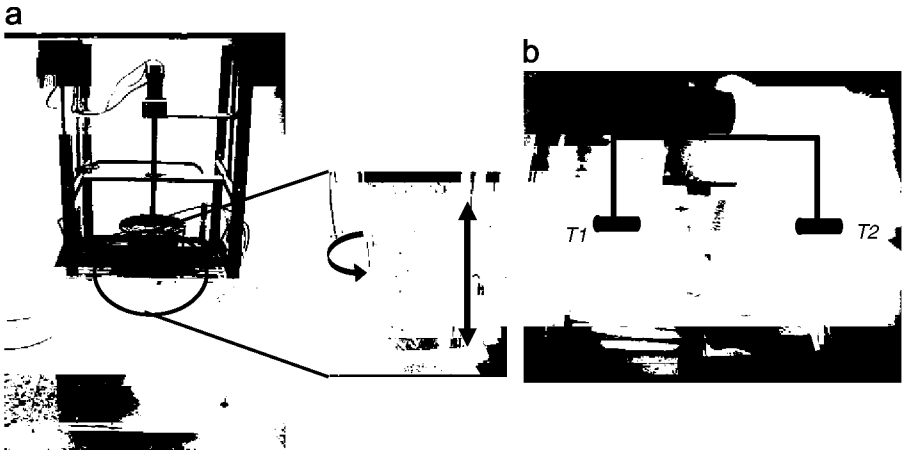

Fig. 2. Ultrasonic inspections: (a) radial scanning and (b) axial scanning.

4.3. Ultrasonic axial scanning (immersion inspections)

For axial scanning (see Fig. 2b), a standard automatic system (with three Cartesian axes) was used. Samples were aligned at the bottom of the tank and two ultrasonic transducers (the same as those used in radial scanning) scanned the parallel surfaces of the samples with a spatial resolution of 4 mm in the horizontal and vertical directions (approximately 600 A-scans in each slice, with a frequency sampling of 20 MHz). Velocity and attenuation maps were generated for each of the slices of the HA-30/00-2 sample. Thus, each pixel of the image corresponds to the ultrasonic information related to a coaxial axis with the revolution axis of the specimen.

5. Results and discussion

5.1. Ultrasonic contact measurements

The ultrasonic contact velocities before (V_0) and after (V_f) the accelerated F–T cycles, the RDME, and the corresponding relative ultrasonic velocities ($RV=V_f/V_0$) for the specimens without and with air-entraining agents are outlined in Tables 3 and 4, respectively. In both specimen groups, variations in velocity before and after the F–T cycles can be observed. It can be seen that for most of the specimens without air-entraining agents, the ultrasonic velocity decreased after the F–T cycles, while in specimens with air-entraining agents, the behavior was the opposite. However, it is worth noting that velocities in some samples (HA-30/00-1 and HA-30/00-4) increased after cycles. This is due to the fact that all samples were cured for 28 days in conditions of low relative humidity; hence, the hydration process was not fully achieved. This behavior was also observed in samples HA-30/00-0 and HA-30/05-0, which were not subjected to F–T cycles. This behavior was confirmed by determination of the relative degree of hydration (before and after the cycles) in the concrete samples without and with air entraining, resulting in 1.1 and 1.3, respectively [24].

It must be noted that the RDME did not reach a critical value (60%); therefore, it is equal to the durability factor (D) according to the standard [6], because $N=300$, as stated in Eq. (1). Table 3 shows that both the RDME and RV indicate that the HA/30-00-2 and HA/30-00-3 specimens were the most damaged, but the Rilem and ASTM criteria differ in the damage classification as described in Table 1. For instance, the HA/30-00-2 and HA/30-00-3 specimens, according to the Rilem recommendation, have been severely deteriorated, whereas the standard ASTM states that they have passable frost resistance; therefore, it reveals that the Rilem criterion is more restrictive than the ASTM criterion. With regard to specimens with air-entraining agents (see Table 4), both RV and RDME indicate that all specimens were not deteriorated according to the Rilem recommendation, or they had frost resistance as indicated by the standard ASTM.

5.2. Ultrasonic radial images

The ultrasonic images before and after the F–T cycles in concrete specimens without and with air-entraining agents are shown in Figs. 3 and 4, respectively. Figs. 3a and b, and 4a and b show the attenuation images, whereas Figs. 3c and d, and 4c and d show the velocity images. It must be noted that rows (a) and (c) in both figures correspond to the ultrasonic inspections performed before starting the F–T cycles, and rows (b) and (d) correspond to applying 300 F–T cycles. In all the images corresponding to ultrasonic inspections before the cycles, the non-uniformity of the specimens can be appreciated within the same group. Moreover, in the images corresponding to the ultrasonic inspections after the cycles, the extension of the damaged zones can be estimated. For example, estimations of the extension of damage from the bottom of the specimens without air entraining can vary between 40 and 70 mm (see Fig. 3).

The ultrasonic information reveals some features concerning this type of deterioration (Fig. 3). In these images, it can be observed that the damage was not equal in all the specimens. For example, the images corresponding to the HA-30/00-1 and HA-30/00-2 specimens show that before the cycles, they were very similar, but after the F–T cycles, the damaged zones were different. In addition, how the damage has progressed from the parallel faces (upper and lower faces) to the center of the specimens can also be observed. Moreover, it can be noted that the attenuation significantly increased when the specimens were subjected to the F–T cycles. Furthermore, there were zones where the ultrasonic waves were not able to go through, and therefore, it was not possible to measure their velocities.

The inability to measure the ultrasonic velocity in some zones of the specimens was due to the fact that the energy of the corresponding received ultrasonic signals did not overcome the defined threshold of measure, (e.g. 1% of maximum normalized signal amplitude) even though both the amplitude maximum of reception system (80 dB) and the maximum energy of the emission pulse (400 V) were employed. It is worth noting that the scanning data were obtained using high frequency broadband transducers (i.e. 500 kHz) because they provided a better lateral

Table 3
Ultrasonic contact velocity in specimens without air-entraining agents.

Specimens	HA-30/00-0	HA-30/00–1	HA-30/00–2	HA-30/00–3	HA-30/00–4	HA-30/00–5	HA-30/00–6
V_0 (m/s)	4500	4460	4390	4360	4300	4480	4430
V_f (m/s)	4620	4480	3880	3730	4410	4270	4210
RV (%)	102.67	100.45	88.38	85.55	102.56	95.31	95.03
RDME (%)	105.40	100.90	78.11	73.19	105.18	90.84	90.31

Table 4
Ultrasonic contact velocity in specimens with air-entraining agents.

Specimens	HA-30/05-0	HA-30/05-1	HA-30/05-2	HA-30/05-3	HA-30/05-4	HA-30/05-5	HA-30/05–6
V_0 (m/s)	4260	4250	4300	4340	4270	4270	4210
V_f (m/s)	4470	4410	4450	4480	4410	4460	4430
RV (%)	104.93	103.76	103.49	103.22	103.28	104.45	105.22
RDME	110.10	107.67	107.10	106.56	106.67	109.10	110.72

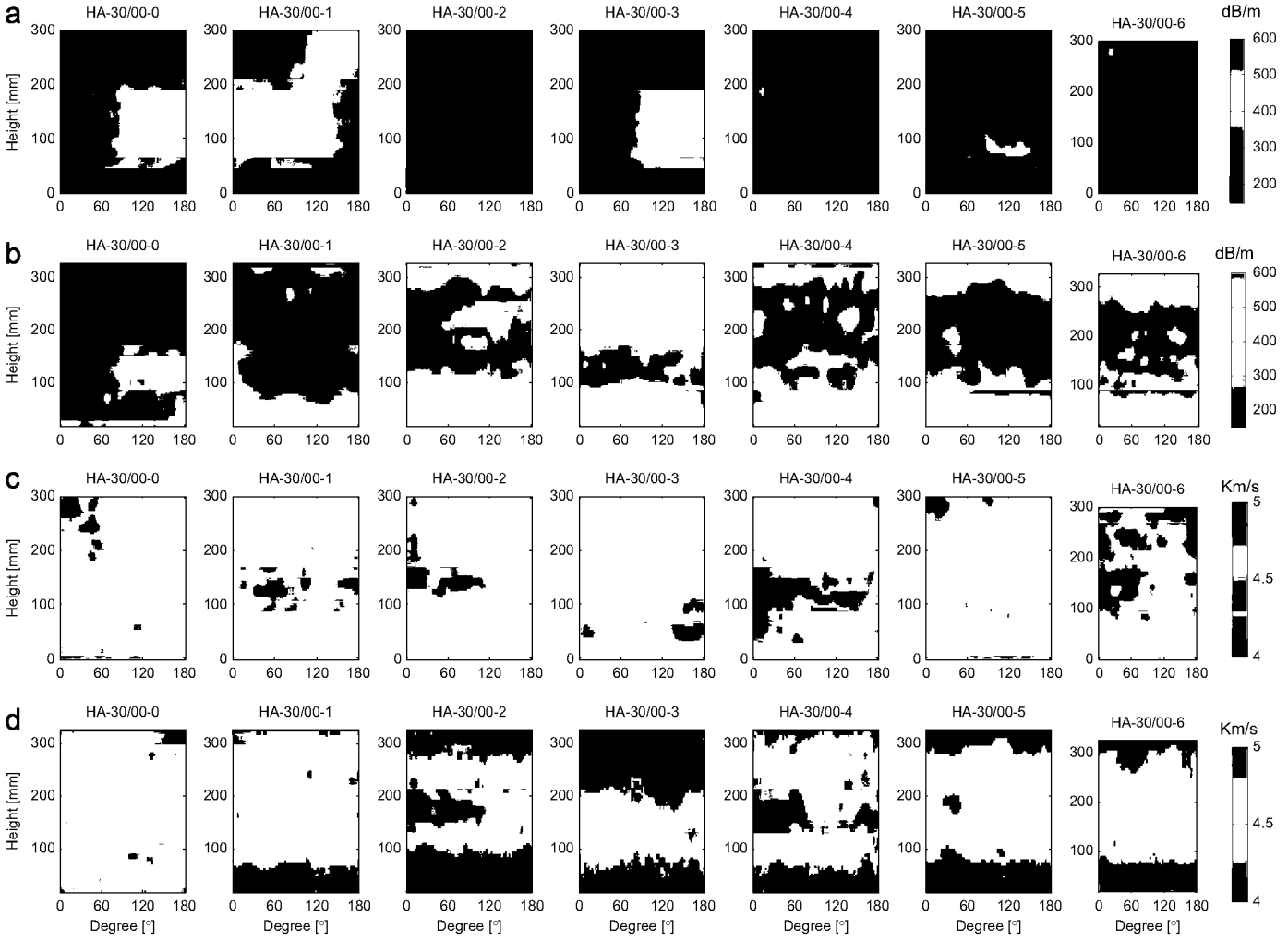

Fig. 3. Ultrasonic images for concrete specimens without air entraining: (a) and (b) attenuation before and after applying the F–T cycles, respectively; (c) and (d) velocity before and after applying the F–T cycles, respectively.

resolution in comparison with other frequency transducers tested (e.g. 54 kHz and 180 kHz) in order to generate the ultrasonic images in the concrete samples. While it is usual to employ low frequency transducers to face the high attenuation involved in common UPV testing (e.g. < 100 kHz), the ultrasonic system used performs through-transmission inspections using immersion coupling allowing, on one hand, much more repetitive measures than direct coupling through gel, and on the other hand, working with higher frequency transducers (e.g. 500 kHz), offering better lateral resolution in the generation of ultrasonic images of the concrete specimens. Furthermore, the freeze–thaw standards require saturation of the samples before applying the trials so that performing ultrasonic inspections in immersion accomplishes such conditions.

On the other hand, Fig. 4 shows images of the concrete specimens with air-entraining agents. In this case, the behavior of the attenuation and the velocity is in contrast to the results corresponding to the concrete specimens without air-entraining agents; the attenuation decreases and the velocity increases. This behavior was also observed in the sample not subjected to F–T cycles, HA-30/05-0, which was stored in a climatic chamber. None of the specimens deteriorated during the cycles, so that the effectiveness of adding air-entraining agents to prolong the durability of the concrete subjected to F–T cycles was verified. In both Figs. 3 and 4, it can be noted that the velocity is increased in the assessable area. This is because all samples were cured for only 28 days in conditions of low relative humidity; hence, the hydration process was not fully achieved [26,27].

One parameter was proposed for our experimental setup, the non-assessable area proportion (NAAP), which is defined as the area proportion where the ultrasonic signal could not travel through the specimen, so that NAAP corresponds to the case where the transmitted signal is too weak to be measured. Thus, the NAAP is obtained by selecting a segmentation threshold in terms of attenuation which is equivalent to the dynamic range of our measurements (80 dB). This dynamic range could be changed in order to improve the experiment conditions. In this experiment, values in attenuation above 350 dB/m are considered as non-assessable areas in which the velocity cannot be determined.

For other experimental setups, the segmentation threshold for the calculation of the NAAP could be chosen by taking into account the attenuation average obtained from ultrasonic attenuation images of sound concrete samples (e.g. before the cycles). For instance, the segmentation threshold can be defined as the attenuation average plus two or three times the deviation standard of the attenuation average value. This suggestion was tested taking into account variations in the segmentation threshold ranging from 240 to 300 dB/m (i.e. variations around 20%), obtaining a maximum change in the NAAP below 5% for one sample (HA-30/001), but for the rest of the samples, changes in the NAAP lower than 2% were observed. Furthermore, using the ultrasonic images, both RV and RDME can be calculated. It must

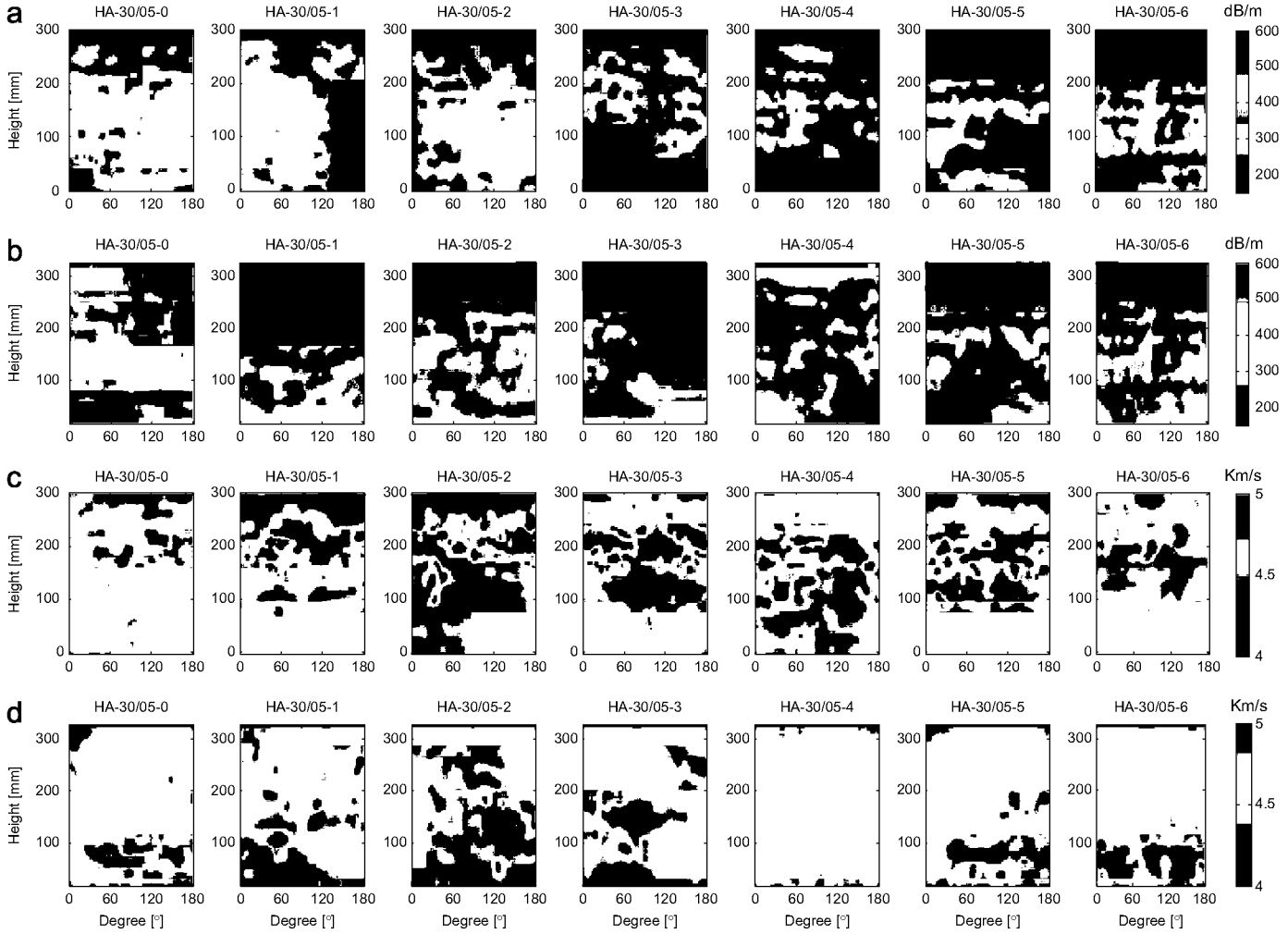

Fig. 4. Ultrasonic images for concrete specimens with air entraining: (a) and (b) attenuation before and after applying the F–T cycles, respectively; (c) and (d) velocity before and after applying the F–T cycles, respectively.

Table 5
Evaluation parameters of damage from ultrasonic images in concrete without air-entraining agents.

Specimens	**HA-30/00-0**	HA-30/00–1	**HA-30/00–2**	**HA-30/00–3**	**HA-30/00–4**	**HA-30/00–5**	**HA-30/00–6**
V_0 (m/s)	4722 ± 212	4683 ± 223	4716 ± 225	4752 ± 93	4752 ± 158	4720 ± 231	4730 ± 79
V_f (m/s)	4725 ± 62	4746 ± 119	4695 ± 135	4665 ± 95	4660 ± 100	4732 ± 111	4684 ± 192
NAAP (%)	0	16.47	44.38	61.03	24.15	36.12	33.83
RV (%)	100.06	101.34	99.55	98.17	98.06	100.25	99.03
RDME	100.13	102.7087	99.11	96.37	96.16	100.51	98.06
V_{ff}/V_0 (%)	100.06	97.83	90.88	87.08	93.70	92.94	92.59
$(V_{ff}/V_0)^2$ (%)	100.13	95.71	82.59	75.83	87.80	86.38	85.73

Table 6
Evaluation parameters of damage from ultrasonic images in concrete with air-entraining agents.

Specimens	**HA-30/05-0**	**HA-30/05-1**	**HA-30/05-2**	**HA-30/05-3**	**HA-30/05-4**	**HA-30/05-5**	**HA-30/05–6**
V_0 (m/s)	4586 ± 226	4556 ± 226	4602 ± 232	4560 ± 226	4740 ± 107	4643 ± 227	4589 ± 132
V_f (m/s)	4650 ± 102	4651 ± 114	4663 ± 104	4663 ± 103	4772 ± 102	4696 ± 98	4634 ± 99
NAAP (%)	0	0.44	0.18	0.47	1.21	0.01	0.30
RV (%)	101.40	102.09	101.33	102.26	100.68	101.14	100.98
RDME	102.81	104.21	102.67	104.57	101.35	102.30	101.97
V_{ff}/V_0 (%)	101.40	101.99	101.29	102.15	100.42	101.14	100.92
$(V_{ff}/V_0)^2$ (%)	102.81	104.02	102.59	104.35	100.85	102.29	101.84

be noted that, in this case, V_f and V_0 are the average ultrasonic velocities obtained only from the assessable area in the images, taking into account that before applying the F–T cycles the assessable area corresponds to the whole sample, while after the cycles, this area corresponds to the zone where the ultrasonic signal could travel through the specimen. Tables 5 and 6 show the

results of these parameters obtained for the concrete specimens without and with air-entraining agents, respectively. The parameter V_{ff} refers to a weighted average velocity in terms of the NAAP and will be explained subsequently.

It was observed that the specimens without air-entraining agents had irregular deterioration, which resulted in different NAAP values. The least damaged was the HA-30/00-1 specimen with an NAAP of 16.47%, and the most damaged was the HA-30/00-3 specimen with an NAAP of 61.03%. However, the RV and the RDME on the evaluated zone were high, greater than 98% and 96%, respectively. On the other hand, the specimens with air-entraining agents did not exhibit deterioration. This result agrees with the RV and the RDME obtained from the contact measurements.

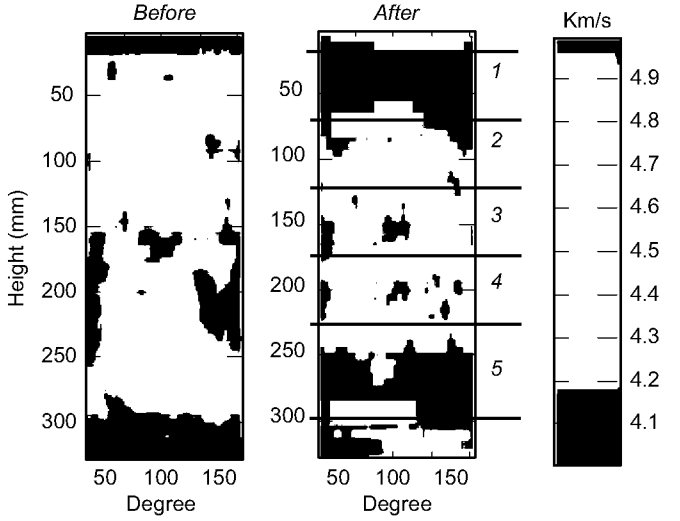

Fig. 5. Radial velocity map (km/s) from the specimen HA-30/00-2 before and after the freeze–thaw cycles.

5.3. Ultrasonic axial images

For an in-depth evaluation of damage by F–T cycles, the sample HA-30/00-2 was selected because it showed a considerable damage in its upper and lower faces; however, it revealed a medium velocity loss in comparison with the rest of the samples. Furthermore, the specimen (HA-30/00-2) did not show any type of cracking or spalling on the surface, as observed in the HA-30/00-3 specimen, where there was material loss. Therefore, specimen HA-30/00-2 was cut into five slices of approximately 50 mm, except Slice 5 (60 mm), as shown in Fig. 5. An axial scanning was performed on these slices so as to analyze and precisely locate the damage in the zones where ultrasonic waves did not go through the material in a radial direction. The images generated (axial velocity and attenuation) concerning the different slices by this inspection are shown in Fig. 6. First, there exist zones on the surface slices of some millimeters thickness, whose velocities were lower than 4.4 km/s as seen in almost all these velocity maps (Fig. 6b). In addition, it can be noted that there is a very high attenuation on Slice 1, indicating that ultrasonic waves were not able to travel through the material in an axial direction in several zones near the surface. Moreover, the attenuation is similar for Slices 2–4, being a little higher in Slice 5, as shown in Fig. 6a.

After calculation of the average velocity in each slice (see V_f in Table 7), it was observed that the velocities in the axial direction of Slices 3 and 4 were almost 3% above the initial average velocity of specimen HA-30/00-2 in the radial direction. The above is because the wave path corresponding to the slices (axial direction scanning) was shorter than that from the specimens scanned in the radial direction, so that more of the high frequency components survive, see Fig. 7, and contribute to the higher velocity measured [28]. Another effect to take into account is the cement hydration brought about by the F–T cycles. As there are no images in the axial direction at zero cycle, the comparison is best performed on Slice 4 (as shown in Table 7 as V_f/V_{f4}) because it has the highest velocity and, therefore, can be considered to be slightly damaged.

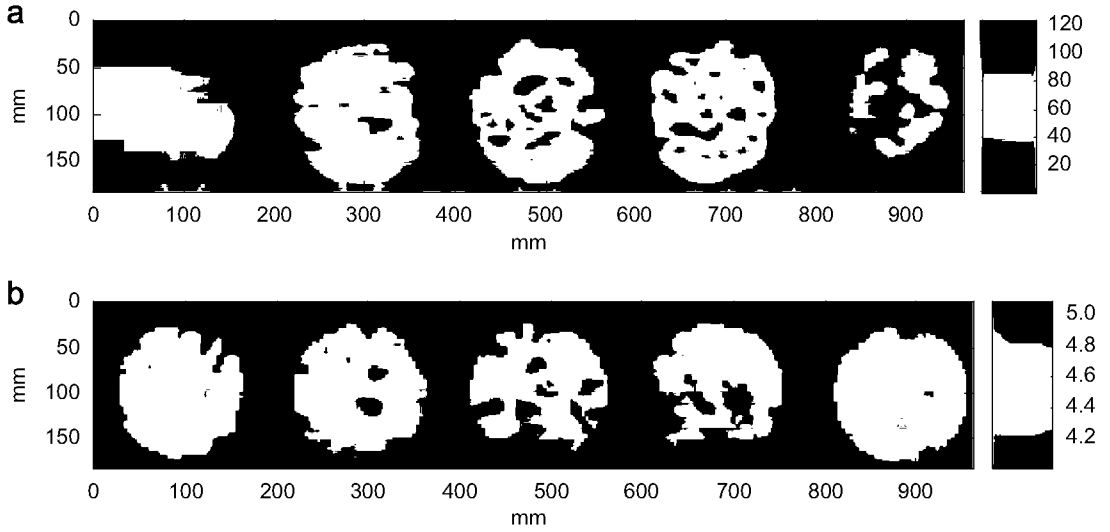

Fig. 6. Axial images from sample HA-30/00-2; these images are arranged from 1 to 5 samples, left to right: (a) attenuation and (b) velocity.

Table 7
Average velocities (m/s) of the slices of the HA-30/00-2 sample.

Slices	1	2	3	4	5
V_f	4562.3 ± 86	4754.9 ± 71	4845.7 ± 86	4856.7 ± 87	4775.8 ± 95
V_f/V_{f4} (%)	93.95	97.92	99.8	100.0	98.35

The relationship with Slice 4, V_f/V_{f4}, showed a noticeable decrease in velocity in Slice 1, whereas this variation regarding the other slices was minimal. It is worth noting that there is a slight velocity loss in Slice 5, in which there is higher attenuation than in the other slices (see Fig. 6a) and a considerable NAAP value in the radial direction could be observed (see Fig. 5). In several slices, both superficial and internal damages were observed.

5.4. Comparison between failure criteria

The failure criteria of the standards ASTM and Rilem, RDME, and RV were calculated to compare with those obtained using the ultrasonic contact measurements (see Tables 3 and 4). Thus, by comparing the values of the failure criteria shown in Tables 3–6, the average velocity values obtained from ultrasonic images were higher than those obtained by contact measurements. However, it must be noted that the average velocity obtained from the ultrasonic images corresponds only to the assessable area of the specimens. In this respect, the failure criteria (RV and RDME) corresponding to the ultrasonic contact measurements must not be directly compared with those obtained from the ultrasonic images. For this purpose, both the average velocities corresponding to the assessable and the non-assessable area proportions should be taken into account. For instance, instead of calculating the RV and the RDME with the V_f as indicated previously, we have proposed another parameter as a weighted average velocity in terms of the NAAP, defined as

$$V_{ff} = \beta V_0 \times \mathrm{NAAP} + V_f(1-\mathrm{NAAP}) \quad (6)$$

where β is a constant value and refers to a given failure percentage. A value of $\beta=0.8$ was considered according to the deterioration degree of the specimen proposed by the Rilem criterion.

Thus, the RV and the RDME can be recalculated using V_{ff}/V_0 and $(V_{ff}/V_0)^2$, respectively. These values are outlined in Tables 6 and 7. As a result, it can be seen that by recalculating these parameters and taking into account the average velocity in both quotients, the values obtained for most of the cases did not differ significantly with respect to those obtained by the ultrasonic contact measurements, as shown in Fig. 8.

In summary, we conclude that the images provide a view of the extension of the damage in F–T experiments. For the evaluation of damage in specimens that were heavily damaged or completely healthy, there were no significant differences between the results obtained with usual parameters of contact measurements, RV or RDME, and those obtained from the images (see Table 8). However, the principal advantage of the use of ultrasonic images is the detection when the damage is incipient (e.g. HA-30/00-1 and HA-30/00-4); in these cases, the contact measurements were not able to detect or quantify it.

In addition, we can observe that by using RDME (either in contact or immersion), the evaluation of damage was a little restrictive because it was classified as frost-resistant for most of the cases, when, in fact, the specimens were actually damaged.

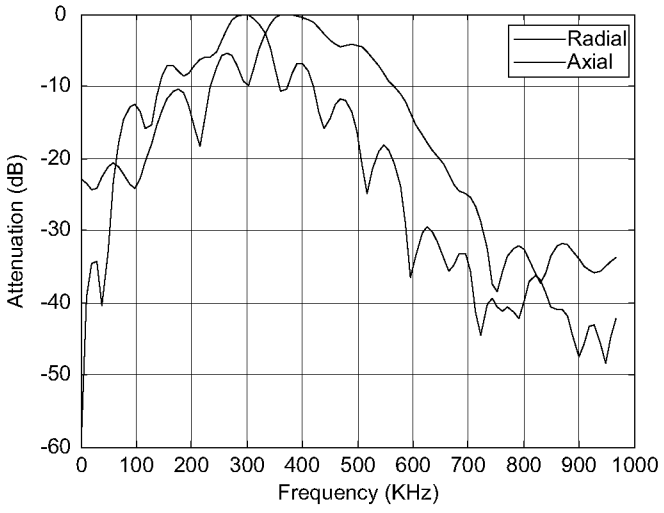

Fig. 7. Comparison of frequency content of signals from radial and axial scanning.

6. Concluding remarks

In this study, the use of ultrasonic imaging as an evaluation tool in concrete subjected to F–T cycles was evaluated. Two groups of concrete specimens, one of them with air-entraining agents, were subjected to accelerated F–T cycles, and the specimens were inspected before and after the cycles by measuring both contact and immersion ultrasonic inspections. Automated ultrasonic radial scanning systems in immersion were designed and used to perform precise measurements and optimize the number, distribution and duration of inspection with capabilities for performing in-situ inspections of cylindrical specimens avoiding the need to take them to a laboratory. With these systems, velocity and attenuation maps could be generated, with which it is possible to quantify the extent of damage. From these ultrasonic images, two parameters have been proposed for these systems to evaluate the damage in the concrete specimens—the NAAP and a weighted average velocity in terms of the NAAP. In view of the obtained results, it could be considered that the NAAP could be related to surface scaling, whereas the weighted average velocity

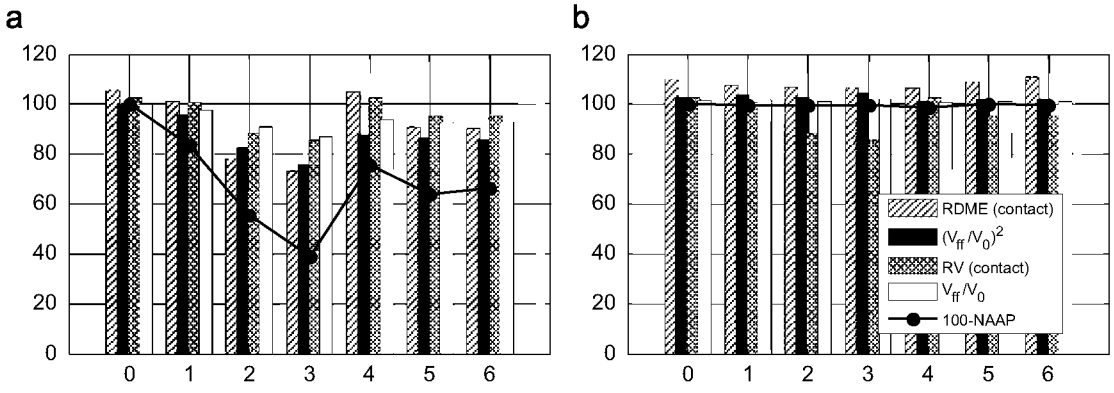

Fig. 8. Comparison between parameters extracted from contact measurements and ultrasonic images.

Table 8
Comparison between failure criteria of ultrasonic contact measurements and ultrasonic imaging evaluation.

Criteria	HA-30/00–1	HA-30/00–2	HA-30/00–3	HA-30/00–4	HA-30/00–5	HA-30/00–6
RV	Not deteriorated	Deteriorated	Deteriorated	Not deteriorated	Possibly deteriorated	Possibly deteriorated
V_{ff}/V_0	Possibly deteriorated	Deteriorated	Deteriorated	Possibly deteriorated	Possibly deteriorated	Possibly deteriorated
RDME	Frost resistant	With passable frost resistant	With passable frost resistant	Frost resistant	Frost resistant	Frost resistant
$(V_{ff}/V_0)^2$	Frost resistant	Frost resistant	With passable frost resistant	Frost resistant	Frost resistant	Frost resistant

could be related to internal damage. The reason that supports the above-mentioned conclusions is twofold. First, the most commonly used parameter to evaluate superficial damage by F–T cycles is scaling, as indicated in different standards. We have thus proposed a parameter, the NAAP, to evaluate this type of damage by means of ultrasonic non-destructive testing. Second, the relative velocity is a parameter used by other standards, but the use of the ultrasonic images provides a complete and more effective evaluation of concrete specimens. However, it must be noted that NAAP depends on the specific setup (sensor sensitivity, frequency), and the geometrical conditions (specimen diameter, total path length); therefore, it could not be used as an absolute parameter. While ultrasonic images inspections in immersion need the extraction of specimens as they were used in this work, one advantage of the proposed parameters and the use of ultrasonic imaging systems like the proposed one is the detection of incipient damage and an alternative evaluation for concrete specimens subjected to F–T cycles.

Acknowledgments

The Spanish Science and Innovation Ministry supported this research under Grant no. BIA 2009-14395-C04-01. S. Aparicio was supported by the postdoctoral JAE-Doc program (CSIC). We also thank the anonymous reviewers for their comments.

References

[1] Mehta PK, Monteiro PJM. Concrete: microstructure, properties, and materials. 3rd ed.. McGraw-Hill; 2006.
[2] Power TC. The physical structure and engineering properties of concrete. Bulletin 90. Skokie, IL: Portland Cement Association; 1958.
[3] Powers TC, Helmuth RA. Theory of volume changes in hardened Portland cement paste during freezing. Highw Res Board Bull 1953;32:285–97.
[4] Setzer MJ. Micro-ice-lens formation in porous solid. J Colloid Interface Sci 2001;243:193–201.
[5] UNE-CEN/TS 12390-9:2008 EX. Testing hardened concrete—part 9: freeze–thaw resistance—scaling. AENOR, 2008.
[6] ASTM C 666/C 666M—03. Standard test method for resistance of concrete to rapid freezing and thawing. American Society of Testing and Materials, 2003.
[7] prENV 12390-9—Testing hardened concrete—part 9: freeze–thaw resistance—scaling. Budapest: European Committee for Standardization; 2003.
[8] JIS A 1148:2001. Method of test for resistance of concrete to freezing and thawing. Japanese Industrial Standards; 2001.
[9] Tang L, Petersson PE. Test-freeze/thaw resistance of concrete—internal deterioration. Mater Struct 2001;34:526–31.
[10] Setzer MJ. CIF-test-capillary suction, internal damage and freeze thaw test reference method and alternative methods A and B. Mater Struct 2001;34:515–21.
[11] SS 13 72 44 Concrete testing—hardened concrete—scaling at freezing. Swedish Standards Institution, 1995.
[12] Selleck SF, Landis EN, Peterson ML, Shah SP, Achenbach JD. Ultrasonic investigation of concrete with distributed damage. ACI Mater J 1998;95: 27–36.
[13] Schickert M. Progress in ultrasonic imaging of concrete. Mater Struct 2005;38:807–15.
[14] Krause M, Milmann B, Mielentz F, Streicher D, Redmer B, Mayer K, et al. Ultrasonic imaging methods for investigation of post-tensioned concrete structures: a study of interfaces at artificial grouting faults and its verification. J Nondestruct Eval 2008;27:67–82.
[15] Schickert M, Tümmler U, Bühling L. Rapid scanning approaches for ultrasonic imaging of concrete. In: Proceedings of the 9th European Conference on NDT (ECNDT), Berlin, 2006.
[16] Chai HK, Aggelis DG, Momoki S, Kobayashi Y, Shiotani T. Single-side access tomography for evaluating interior defect of concrete. Constr Build Mater 2010;24:2411–8.
[17] Hernández MG, Anaya JJ, Sanchez T, Segura I. Porosity estimation of aged mortar using a micromechanical model. Ultrasonics 2006;44:e1007–11.
[18] Segura I, Moragues A, Macphee DE, Anaya JJ, Molero M. Study of the decalcification process in mortars degraded by NH_4NO_3 by using ultrasonic techniques. Mater Constr. 2009;59:17–36.
[19] Molero M, Segura I, Izquierdo MAG, Fuente JV, Anaya JJ. Sand/cement ratio evaluation on mortar using neural networks and ultrasonic transmission inspection. Ultrasonics 2009;49:231–7.
[20] Molero M, et al. Portable non-destructive testing system for cementitious samples with axial symmetry by using ultrasonic imaging and associated procedure. Patent PCT/ES2011/070499.
[21] Ohtsu M. Nondestructive evaluation of damaged concrete due to freezing and thawing by elastic-wave method. J Adv Concr Technol 2005;3:333–41.
[22] Zaharieva R, Buyle-Bodin F, Wirquin E. Frost resistance of recycled aggregate concrete. Cem Concr Res 2004;34:1927–32.
[23] UNE-EN 12390–2:2009. Testing hardened concrete—part 2: making and curing specimens for strength tests. AENOR, 2009.
[24] Al-Assadi G, Casati MJ, Fernández J, Gálvez JC. Effect of the curing conditions of concrete on the behavior under freeze–thaw cycles. Fatigue Fract Eng Mater Struct 2010;32:461–9.
[25] Molero M, Izquierdo MAG, Anaya JJ.. Caracterización de materiales mediante la dispersión ultrasónica: aplicación a los materiales cementicios. Ed. Académica Española, 2011, ISBN: 978-3-8443-4134-8 (in spanish).
[26] Massaza F. Pozzolana and pozzolanic cements. In: Hewlett PC, editor. Lea's chemistry of cement and concrete. Oxford: Elsevier; 1998. p. 471–602.
[27] Segura I, Sánchez E, Moragues A, Hernández MG. Assessment of mortar evolution in pig slurry by mechanical and ultrasonic measurements. Constr. Build Mater 2010;24(9):1572–9.
[28] Chaix JF, Garnier V, Corneloup G. Ultrasonic wave propagation in heterogeneous solid media: theoretical analysis and experimental validation. Ultrasonics 2006;44:200–10.